Domain-Wall Tunneling Electroresistance Effect

M. Li

L. L. Tao

Evgeny Y. Tsymbal

Domain-Wall Tunneling Electroresistance Effect

M. Li, L. L. Tao,[*] and Evgeny Y. Tsymbal[†]

*Department of Physics and Astronomy & Nebraska Center for Materials and Nanoscience,
University of Nebraska, Lincoln, Nebraska 68588, USA*

Ferroelectric tunnel junctions (FTJs) utilizing an in-plane head-to-head ferroelectric domain wall (DW) have recently been realized, showing interesting physics and new functionalities. However, the DW state in these junctions was found to be metastable and not reversible after applying an electric field. In this work, we demonstrate that a stable and reversible head-to-head DW state can be achieved in FTJs by proper engineering of polar interfaces. Using density functional theory (DFT) calculations and phenomenological modeling, we explore the DW stability by varying stoichiometry of the $La_{1-x}Sr_xO/TiO_2$ interfaces in FTJs with $La_{0.5}Sr_{0.5}MnO_3$ electrodes and a ferroelectric $BaTiO_3$ tunnel barrier. For, $x \leq 0.4$ we find that the DW state becomes a global minimum and the calculated hysteresis loops exhibit three reversible polarization states. For such FTJs, our quantum transport calculations predict the emergence of a DW tunneling electroresistance effect—reversible switching of the tunneling conductance between the highly conductive DW state and two much less conductive uniform polarization states.

Ferroelectric tunnel junctions (FTJs) have aroused significant interest due to the rich physics controlling their electronic and transport properties and promising technological applications as nanoscale resistive switching devices [1–3]. A FTJ consists of two metal electrodes separated by a nm-thick ferroelectric barrier which allows electron tunneling through it. The key property is tunneling electroresistance (TER) that is a change in resistance of a FTJ with reversal of ferroelectric polarization. Following the theoretical predictions [4,5], there have been a number of successful experimental demonstrations of the TER effect in trilayer junctions [6–11]. The structural and/or electronic asymmetry of the FTJ is known to play a decisive role for the TER effect. It is now generally accepted that the sizable TER effect can be achieved by using dissimilar electrodes [12–14] through interface engineering [15–20], applied bias [21,22], or defect control [23,24]. Contrary to ferroelectric capacitors where leakage currents are detrimental to the device performance, the conductance of a FTJ is the functional characteristic of the device [25]. This makes FTJs promising for nonvolatile memory applications [26,27].

Very recently, Sanchez-Santolino *et al.* [28] realized a different type of FTJ where ferroelectric polarization forms an in-plane domain wall (DW). In general, ferroelectric DWs are regions separating uniformly polarized domains in ferroelectric materials [29]. There are two types of ferroelectric DWs: neutral DWs, where the normal component of the spontaneous polarization is continuous across the DW, and charged DWs, where a bound charge accumulates at the DW due to discontinuity of the normal component of the polarization. The latter are known as head-to-head DWs (carrying a positive polarization charge) or tail-to-tail DWs (carrying a negative polarization charge). The charged DWs are often electrically conductive, a property which makes them useful for developing novel electronic devices [30,31].

While the previous work has explored electric conductivity *along* the DW, Sanchez-Santolino *et al.* [28] have demonstrated transport *across* the DW. They succeeded to fabricate FTJs with $La_{1-x}Sr_xMnO_3$ (LSMO) electrodes and a ferroelectric $BaTiO_3$ (BTO) tunnel barrier, where ferroelectric polarization of BTO formed an in-plane head-to-head DW. Such a charged DW within the nm-thick barrier layer was stabilized by a confined electron gas formed at the DW, which allowed studying tunneling conduction across it.

The realization of a DW-FTJ is interesting due to the polarization ordering different from uniform. Such ordering supports resonant tunneling across a quantum well formed at the DW, which strongly enhances the FTJ conductance. [28,32] Our follow-up theoretical work has demonstrated that a head-to-head DW structure in LSMO/BTO/LSMO FTJs was induced by polar interfaces, and the resonant tunneling mechanism through the confined electron gas was confirmed by quantum-transport calculations, revealing strongly enhanced conductance of the DW-FTJ [33]. We found, however, that the total energy of the DW state was higher than that of the uniform polarization (UP) state, indicating that the DW state was metastable. This behavior was consistent with the experimental observations by Sanchez-Santolino *et al.* [28], who found that once a DW was destroyed by applying a sufficiently large electric field, it could not be restored. It would be highly desirable to find conditions at which the DW state represented a global minimum, so that the FTJ could be reversibly switched between an UP state and a head-to-head DW

state by applying an electric field. In addition to the enhanced DW-state conductance, such a DW-FTJ could exhibit three nonvolatile resistance states—two corresponding to the UP states and one corresponding to the DW state.

In this paper, we demonstrate that by proper engineering of polar interfaces in a FTJ, a head-to-head DW state can be stabilized as the ground state in a nm-thick ferroelectric barrier layer. This property allows reversible switching between UP and DW states in the DW-FTJ, resulting in a DW-TER effect. To illustrate this concept, we consider a FTJ with LSMO electrodes and a BTO barrier layer, where the $La_{1-x}Sr_xO/TiO_2$ interface stoichiometry controls the DW state. By performing first-principles calculations, we show that a head-to-head DW can be turned into a global energy minimum state separated by energy barriers from the UP states. Using a phenomenological model, we demonstrate a polarization hysteresis loop exhibiting reversible transitions between the UP states and the DW state under an applied electric field. Our quantum-transport calculations reveal that the DW state has many orders in magnitude higher transmission as compared to the UP states, which manifests the DW-TER effect. For asymmetric interface doping, we find that the DW-FTJ exhibits three nonvolatile resistance states.

First, we explore conditions for stabilizing a DW state in a FTJ by controlling interface stoichiometry. The FTJ consists of $La_{0.5}Sr_{0.5}MnO_3$ electrodes and a BTO tunnel barrier stacked along the [001] direction [Fig. 1(a)]. Following the experimental results [28], we consider the $La_{1-x}Sr_xO/TiO_2$ termination at both interfaces and fix $La_{0.5}Sr_{0.5}MnO_3$ and BTO layer thickness at 7.5 and 11.5 unit cells (u.c.), respectively. The interface stoichiometry is determined by the interface Sr doping x, which for now we assume to be the same at both interfaces. Density-functional theory (DFT) calculations are performed using the plane-wave ultrasoft pseudopotential method [34] implemented in Quantum ESPRESSO [35], as described in the Supplemental Material [36].

We find that in all the explored range of interface stoichiometries, i.e., $x \leq 0.75$, the DW state can be stabilized in the process of atomic structure relaxation by using proper initial atomic displacements. However, depending on the interface stoichiometry, the DW state represents either a local or global energy minimum. As an example, Figs. 1(a) and 1(b) show the relaxed atomic structure of the FTJ with the $La_{0.9}Sr_{0.1}O/TiO_2$ interface termination ($x = 0.1$) for UP and DW states, respectively. The corresponding metal-oxygen displacement profiles are shown in the Supplemental Material [36], Fig. S1. In this case, the DW state has the lowest energy, i.e., it represents a global energy minimum. However, with the increasing Sr concentration at the interface, the UP state energy becomes lower and eventually the DW state develops into a local energy minimum. This behavior is seen from Fig. 1(c),
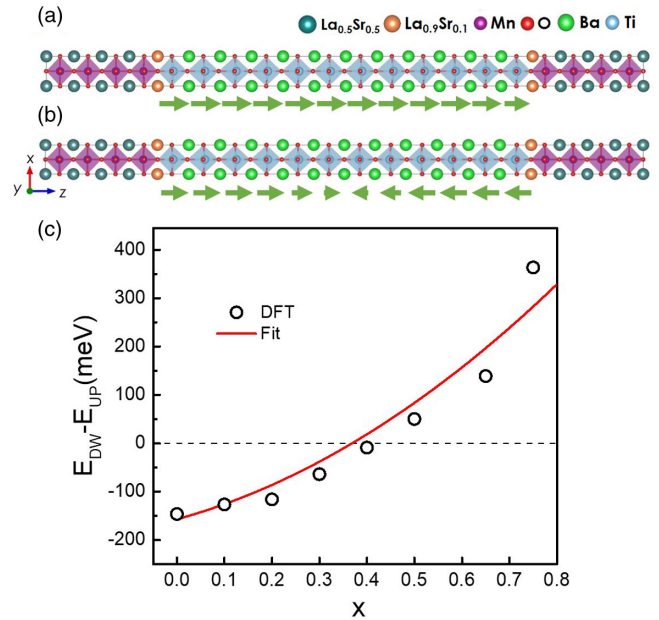

FIG. 1. Relaxed atomic structure of a DW-FTJ for UP (a) and head-to-head DW (b) states for $x = 0.1$. (c) Energy difference (dots) between DW state (E_{DW}) and UP state (E_{UP}) as a function of interface Sr concentration x. Circles: DFT results; line: fitting results using a model described in Supplemental Material [36], Sec. S3.

which shows the calculated energy difference between the DW and UP states as a function of x at the $La_{1-x}Sr_xO/TiO_2$ interface. It is evident that while the UP state is more energetically favorable at larger x, when x is reduced down to $x \leq 0.4$, the DW state becomes a global energy minimum. Clearly, the lower interfacial Sr doping enhances the stability of the DW state.

This dependence on the interface stoichiometry can be qualitatively understood in terms of the interface bound charge supporting the DW state. The nominal ionic charge of $1 - x$ at the interfacial $La_{1-x}Sr_xO$ monolayer increases with decreasing x. This positive bound charge favors polarization pointing away from the interface and thus the DW state. It partly screens the polarization charge at both interfaces and controls the electron density of the two-dimensional electron gas (2DEG), which partly screens the polarization charge at the head-to-head DW [33]. A simple model based on the electrostatic energy of the FTJ, being determined by the ionic surface charge density at the two interfaces, the polarization charge density at the interfaces and DW, the band offset between the electrodes and ferroelectric, the formation of the 2DEG at the DW, and screening in the electrodes, allows a reasonable fit of the DFT results, as shown in Fig. 1(c) by the solid line (see Sec. S3 in Ref. [36] for details).

The formation of the energy minima at the DW and UP states can be analyzed using a polarization-dependent energy profile. Following the previously developed procedure [42], we perform total energy calculations for

different atomic structures of the FTJ, which are obtained by interpolating between the DW state and the two opposite UP states (polarized left or right). The z coordinates of atom m for DW, left-UP and right-UP states, z_m^{DW}, z_m^L, and z_m^R, respectively, can be parametrized by dimensionless parameter λ as follows:

$$z_m(\lambda) = \begin{cases} (1-\lambda)z_m^{DW} + \lambda z_m^R, & 0 \le \lambda \le 1 \\ \frac{1}{2}(\lambda+1)z_m^R - \frac{1}{2}(\lambda-1)z_m^L, & \lambda > 1 \\ (1+\lambda)z_m^{DW} - \lambda z_m^L, & -1 \le \lambda \le 0 \\ \frac{1}{2}(\lambda+1)z_m^R - \frac{1}{2}(\lambda-1)z_m^L, & \lambda < -1 \end{cases}, \quad (1)$$

where $\lambda = -1$, $\lambda = 0$, and $\lambda = +1$ correspond to the left-UP, DW, and right-UP states, respectively. Figure 2 shows that independent of x, there are three energy minima corresponding to the DW state ($\lambda = 0$) and two UP states ($\lambda = \pm 1$). However, while for $x = 0.1$ and $x = 0.3$ the DW state represents the global energy minimum, for $x = 0.5$ it transforms to a local energy minimum. The energy minima are separated by barriers around $\lambda = \pm 0.5$, which stabilize the DW and UP states.

Next, we develop a simple phenomenological model to demonstrate a possibility of reversible switching between the DW and UP states. For the UP state, we assume that the polarization is constant across the whole BTO layer. For the DW state, we assume that the polarization is constant in each monodomain region (P_1 and P_2) but changes linearly across the DW region [Fig. 3(a)], which is line with our DFT calculations (Fig. S1 in the Supplemental Material
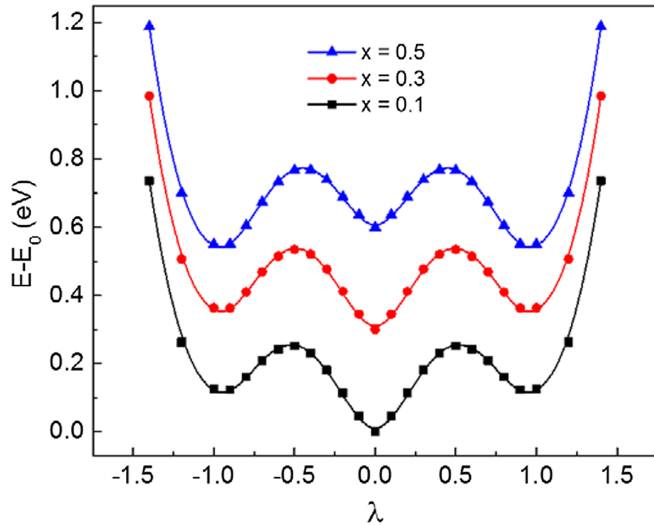
[36]). Using this approximation, the Ginzburg-Landau-Devonshire free energy for a FTJ can be expressed as [43,44]

$$F(P_1, P_2) = F_0 + \frac{A}{2}(P_1^2 + P_2^2) + \frac{B}{4}(P_1^4 + P_2^4) + K(P_1 - P_2) + G(P_1 - P_2)^2, \quad (2)$$

where F_0 is a reference energy, the A and B dependent terms represent bulk (and interface) contributions, the K dependent term accounts for the linear in P contributions from the two interfaces which by symmetry have an opposite sign, and the G-dependent term is proportional to the polarization charge squared in the DW region. According to Eq. (1), polarizations P_1 and P_2 can be expressed in terms of dimensionless parameter λ so that [36]

$$F(\lambda) = c + f(1 - \lambda_1 + \lambda_1|\lambda|) + f(\lambda_1 + |\lambda| - \lambda_1|\lambda|) + \xi(1 - |\lambda|) + \gamma(1 - |\lambda|)^2, \quad (3)$$

where $|\lambda| < 1$ and $f(x) = \frac{1}{2}\alpha(2x-1)^2[(2x-1)^2 - 2]$. For $|\lambda| > 1$ corresponding to the uniform polarization, Eq. (3) is reduced to $F(\lambda) = f(\frac{1}{2} + \frac{1}{2}\lambda)$. We use these equations to fit the DFT calculated energy profiles, where $c, \alpha, \lambda_1, \xi,$ and γ are considered as fitting parameters. As is seen from Fig. 2, the DFT results are perfectly described by the simple
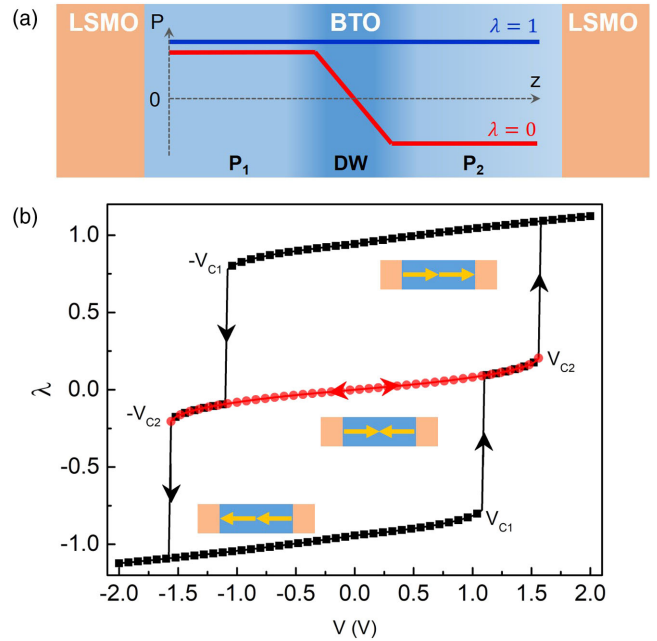

(a)

(b)

FIG. 3. (a) Polarization profile assumed within the phenomenological model for the DW state (red) and in the UP state (blue). (b) Simulated hysteresis loop for $x = 0.1$ based on the phenomenological model. Red dots indicate the DW state. Insets: schematic representation of different polarized states. V_{C1} and V_{C2} denote coercive voltages.

FIG. 2. Total energy (with respect to the DW state) as a function of interpolation parameter λ calculated from DFT calculations (symbols) and fitted using the phenomenological model (lines). Black, red, and blue plots correspond to $x = 0.1$, $x = 0.3$ (with an offset of 0.3 eV) and $x = 0.5$ (with an offset of 0.6 eV), respectively. Notice that $\lambda = 0$ and $\lambda = \pm 1$ correspond to the DW and UP states, respectively.

phenomenological model. The obtained fitting parameters are listed in Supplemental Material [36], Table S1.

To simulate a hysteresis loop, we add an electrostatic energy term, $-AP_0V\lambda$, [36] to the free energy of Eq. (3), where A is the cross area, P_0 is the saturation polarization, and V is the applied voltage. We change voltage V continuously from negative to positive (and then back), and for each value of V find the local energy minimum nearest (in terms of λ) to that for the preceding value of V. The local minimum is obtained from $\partial F(\lambda, V)/\partial\lambda = 0$ which determines $\lambda(V)$.

Figure 3(b) shows the simulated hysteresis loop based on the phenomenological model. Starting from an initial left UP state (the local energy minimum at $\lambda = -1$ in Fig. 2), the polarization λ increases linear with voltage V up to the coercive voltage V_{C1}, at which the left UP energy minimum vanishes and polarization jumps to the nearest local energy minimum corresponding to the DW state ($\lambda = 0$ in Fig. 2). A further increase of voltage flattens the DW energy minimum and eventually, at $V = V_{C2}$, the polarization switches to the right UP state ($\lambda = 1$ in Fig. 2). A similar behavior occurs when the voltage decreases and polarization switches from the right UP state to the left UP state through the DW state. Thus, the calculated hysteresis loop [shown by a black line in Fig. 3(b)] reveals the appearance of the three polarization states depending on the applied voltage.

Importantly, our modeling demonstrates that the DW state can be stabilized at zero field after applying voltage V, such that $V_{C1} < V < V_{C2}$, and then by reducing it to zero [red curve in Fig. 3(b)]. This, implies that the three polarization states are reversible, and can be experimentally realized by a voltage pulse of proper magnitude and sign. As follows from our modeling, for the considered FTJ, this property holds for $x \leq 0.4$ (Fig. S4 [36]). For, $x > 0.4$ the DW state becomes a local minimum and cannot be restored after the polarization have been saturated [Fig. S4(c) [36]] [45].

As follows from our previous results [33], UP and DW states exhibit significantly different conductance. The DW-state conductance is hugely enhanced due to resonant tunneling across quantum-well states formed at the ferroelectric DW. Thus, using proper polar interface engineering proposed in this work, a giant DW-TER effect can be realized experimentally.

Moreover, a DW-FTJ can be made asymmetric, resulting in a conventional TER effect, which in conjunction with the stable DW state would produce three nonvolatile resistance states. Such DW-FTJ functionality can be achieved using different stoichiometry x of the two polar interfaces. As an example, we consider a DW-FTJ with $x = 0.1$ and $x = 0.3$ at left and right interfaces, respectively. Figures S5 and S6 in the Supplemental Material [36] show the calculated atomic structures and polar displacements. Table I summarizes the calculated total energy and total transmission for

TABLE I. The calculated total energy and transmission for an asymmetric FTJ with $x = 0.1$ at the left interface and $x = 0.3$ at the right interface.

State	Energy (meV)	Transmission
Left UP	155	2.16×10^{-13}
DW	0	8.49×10^{-8}
Right UP	77	3.07×10^{-13}

the DW-FTJ in the three polarization states. It is seen that the DW state is energetically favorable to both UP states. The total energy for the right UP state is slightly lower than that for the left UP state due to the larger positive ionic charge at the left interface, which favors polarization pointing to right. The DW-state transmission is predicted to be nearly 5 orders of magnitude larger than the transmission for the two UP states, and the associated giant DW TER ratio increases exponentially with barrier thickness (Fig. S9 [36]). This designates the DW-TER effect. The transmission for the right UP state is about 50% larger than that for left UP state, which reflects a conventional TER effect.

Figure 4 shows the calculated $\mathbf{k}_{\parallel}$-resolved transmission for the DW-FTJ in the three polarization states. Overall, the transmission landscape is controlled by the $\mathbf{k}_{\parallel}$-profile of the propagating states in the electrodes, the potential barrier height across the BTO barrier, and the presence of quantum-well states [33]. The latter appear in the DW state [Fig. S7(a) [36]] and dominate transmission through resonant tunneling, as seen from Fig. 4(a) (four red arcs and a yellow square around the $\bar{\Gamma}$ point). The transmission spectra for the UP states [Figs. 4(b) and 4(c)] reveal direct tunneling features with significantly lower transmission probabilities compared to the DW state. The slightly reduced transmission over the whole Brillion zone for the left UP state [Fig. 4(c)] compared to the right UP state [Fig. 4(b)] is due to the lower barrier height for the latter, as evident from Figs. S7(b) and S7(c) in the Supplemental Material [36].

The proposed engineering of the polar La$_{1-x}$Sr$_x$O interface is feasible using modern growth techniques such as
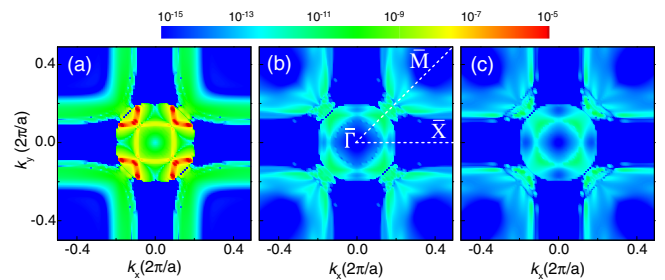

FIG. 4. Calcuated $\mathbf{k}_{\parallel}$-resolved transmission in the two-dimensional Brillouin zone of asymmetric FTJ with $x = 0.1$ at the left interface and $x = 0.3$ at the right interface in the DW state (a), and right UP (b) and left UP (c) states.

pulsed laser deposition. For example, Hikita *et al.* [46] used this technique to systematically study the effect of $La_{0.7}Sr_{0.3}MnO_3/Nb:SrTiO_3$ interface termination on the Schottky barrier height. The insertion of a $SrMnO_3$ monolayer of variable thickness less than a unit cell on the TiO_2 terminated $SrTiO_3$ led to variable stoichiometry of the $La_{1-x}Sr_xO$ interfacial monolayer in the range of $0.3 \leq x \leq 1$. In a similar way, the fractional insertion of a $LaMnO_3$ monolayer on the TiO_2 terminated BTO with follow-up deposition of $La_{0.7}Sr_{0.3}MnO_3$ will lead to the $La_{1-x}Sr_xO$ interfacial monolayer with $0 \leq x \leq 0.3$, as required for the formation of the head-to-head DW. The other interface can be grown in a similar way.

In summary, we have demonstrated a possibility to realize a DW-TER effect—reversible switching of the tunneling conductance between a highly conductive DW state and two much less conductive UP states. The key factor for observing the DW-TER effect is stabilizing a reversible head-to-head DW wall state in a FTJ, which can be achieved by proper engineering of polar interfaces. Using DFT calculations and phenomenological modeling, we have predicted the emergence of this effect in LSMO/BTO/LSMO FTJs with the appropriate $La_{1-x}Sr_xO/TiO_2$ interface stoichiometry, which controls the stability of the DW state. We hope that our results will stimulate experimental efforts to design and explore DW-FTJs exhibiting the DW-TER effect.

*ltao2@unl.edu
†tsymbal@unl.edu

[1] E. Y. Tsymbal and H. Kohlstedt, Science 313, 181 (2006).
[2] V. Garcia and M. Bibes, Nat. Commun. 5, 4289 (2014).
[3] J. P. Velev, J. D. Burton, M. Y. Zhuravlev, and E. Y. Tsymbal, npj Comput. Mater. 2, 16009 (2016).
[4] M. Y. Zhuravlev, R. F. Sabirianov, S. S. Jaswal, and E. Y. Tsymbal, Phys. Rev. Lett. 94, 246802 (2005).
[5] H. Kohlstedt, N. A. Pertsev, J. R. RodriguezContreras, and R. Waser, Phys. Rev. B 72, 125341 (2005).
[6] A. Chanthbouala, A. Crassous, V. Garcia, K. Bouzehouane, S. Fusil, X. Moya, J. Allibe, B. Dlubak, J. Grollier, S. Xavier, C. Deranlot, A. Moshar, R. Proksch, N. D. Mathur, M. Bibes, and A. Barthelemy, Nat. Nanotechnol. 7, 101 (2012).
[7] D. J. Kim, H. Lu, S. Ryu, C.-W. Bark, C.-B. Eom, E. Y. Tsymbal, and A. Gruverman, Nano Lett. 12, 5697 (2012).
[8] Z. Wen, C. Li, D. Wu, A. Li, and N. B. Ming, Nat. Mater. 12, 617 (2013).
[9] H. Lu, A. Lipatov, S. Ryu, D. J. Kim, H. Lee, M. Y. Zhuravlev, C. B. Eom, E. Y. Tsymbal, A. Sinitskii, and A. Gruverman, Nat. Commun. 5, 5518 (2014).
[10] S. Boyn, A. M. Douglas, C. Blouzon, P. Turner, A. Barthelemy, M. Bibes, S. Fusil, J. M. Gregg, and V. Garcia, Appl. Phys. Lett. 109, 232902 (2016).
[11] Z. Xi, J. Ruan, C. Li, C. Zheng, Z. Wen, J. Dai, A. Li, and D. Wu, Nat. Commun. 8, 15217 (2017).
[12] A. Zenkevich, M. Minnekaev, Yu. Matveyev, Yu. Lebedinskii, K. Bulakh, A. Chouprik, A. Baturin, K. Maksimova, S. Thiess, and W. Drube, Appl. Phys. Lett. 102, 062907 (2013).
[13] R. Soni, A. Petraru, P. Meuffels, O. Vavra, M. Ziegler, S. K. Kim, D. S. Jeong, N. A. Pertsev, and H. Kohlstedt, Nat. Commun. 5, 5414 (2014).
[14] L. L. Tao and J. Wang, J. Appl. Phys. 119, 224104 (2016).
[15] Z. Wen, C. Li, D. Wu, A. Li, and N. B. Ming, Nat. Mater. 12, 617 (2013).
[16] J. D. Burton and E. Y. Tsymbal, Phys. Rev. Lett. 106, 157203 (2011).
[17] A. Tsurumaki-Fukuchi, H. Yamada, and A. Sawa, Appl. Phys. Lett. 103, 152903 (2013).
[18] V. S. Borisov, S. Ostanin, S. Achilles, J. Henk, and I. Mertig, Phys. Rev. B 92, 075137 (2015).
[19] L. L. Tao and J. Wang, Appl. Phys. Lett. 108, 062903 (2016).
[20] Q. Yang, L. Tao, Y. Zhang, M. Li, Z. Jiang, E. Y. Tsymbal, and V. Alexandrov, Nano Lett. 19, 7385 (2019).
[21] D. I. Bilc, F. D. Novaes, J. Íñiguez, P. Ordejón, and P. Ghosez, ACS Nano 6, 1473 (2012).
[22] A. Useinov, A. Kalitsov, J. Velev, and N. Kioussis, Appl. Phys. Lett. 105, 102403 (2014).
[23] H. Lu, D. Lee, K. Klyukin, L. Tao, B. Wang, H. Lee, J.-W. Lee, T. R. Paudel, L.-Q. Chen, E. Y. Tsymbal, V. Alexandrov, C. Eom, and A. Gruverman, Nano Lett. 18, 491 (2018).
[24] K. Klyukin, L. L. Tao, E. Y. Tsymbal, and V. Alexandrov, Phys. Rev. Lett. 121, 056601 (2018).
[25] E. Y. Tsymbal and A. Gruverman, Nat. Mater. 12, 602 (2013).
[26] S. Boyn, S. Girod, V. Garcia, S. Fusil, S. Xavier, C. Deranlot, H. Yamada, C. Carrétéro, E. Jacquet, M. Bibes, A. Barthélémy, and J. Grollier, Appl. Phys. Lett. 104, 052909 (2014).
[27] M. Abuwasib, H. Lu, T. Li, P. Buragohain, H. Lee, C.-B. Eom, A. Gruverman, and U. Singisetti, Appl. Phys. Lett. 108, 152904 (2016).
[28] G. Sanchez-Santolino, J. Tornos, D. Hernandez-Martin, J. I. Beltran, C. Munuera, M. Cabero, A. Perez-Muñoz, J. Ricote, F. Mompean, M. Garcia-Hernandez, Z. Sefrioui, C. Leon, S. J. Pennycook, M. C. Muñoz, M. Varela, and J. Santamaria, Nat. Nanotechnol. 12, 655 (2017).
[29] G. Catalan, J. Seidel, R. Ramesh, and J. F. Scott, Rev. Mod. Phys. 84, 119 (2012).
[30] I. Stolichnov, L. Feigl, L. J. McGilly, T. Sluka, X. K. Wei, E. Colla, A. Crassous, K. Shapovalov, P. Yudin, A. K. Tagantsev, and N. Setter, Nano Lett. 15, 8049 (2015).
[31] J. Seidel, L. W. Martin, Q. He, Q. Zhan, Y.-H. Chu, A. Rother, M. E. Hawkridge, P. Maksymovych, P. Yu, M. Gajek, N. Balke, S. V. Kalinin, S. Gemming, F. Wang,

G. Catalan, J. F. Scott, N. A. Spaldin, J. Orenstein, and R. Ramesh, Nat. Mater. **8,** 229 (2009).

[32] E. Y. Tsymbal and J. P. Velev, Nat. Nanotechnol. **12,** 614 (2017).

[33] M. Li, L. L. Tao, J. P. Velev, and E. Y. Tsymbal, Phys. Rev. B **97,** 155121 (2018).

[34] D. Vanderbilt, Phys. Rev. B **41,** 7892(R) (1990).

[35] P. Giannozzi, S. Baroni, N. Bonini, M. Calandra, R. Car, C. Cavazzoni, D. Ceresoli, G. L. Chiarotti, M. Cococcioni, I. Dabo *et al.*, J. Phys. Condens. Matter **21,** 395502 (2009).

[36] See Supplemental Material at http://link.aps.org/supplemental/10.1103/PhysRevLett.123.266602 for computational details, atomic structure, electrostatic model, phenomenological model, and simulated hysteresis loops of symmetric FTJs, atomic, and electronic structures and hysteresis loops of asymmetric FTJs, and thickness dependence of DW TER, which includes Refs. [4,16], and [37–41].

[37] J. P. Perdew, K. Burke, and M. Ernzerhof, Phys. Rev. Lett. **77,** 3865 (1996).

[38] J. D. Burton and E. Y. Tsymbal, Phys. Rev. B **80,** 174406 (2009).

[39] H. J. Choi and J. Ihm, Phys. Rev. B **59,** 2267 (1999).

[40] A. Smogunov, A. Dal Corso, and E. Tosatti, Phys. Rev. B **70,** 045417 (2004).

[41] G. Gerra, A. K. Tagantsev, N. Setter, and K. Parlinski, Phys. Rev. Lett. **96,** 107603 (2006).

[42] X. Liu, Y. Wang, P. V. Lukashev, J. D. Burton, and E. Y. Tsymbal, Phys. Rev. B **85,** 125407 (2012).

[43] R. Kretschmer and K. Binder, Phys. Rev. B **20,** 1065 (1979).

[44] G. Gerra, A. K. Tagantsev, and N. Setter, Phys. Rev. Lett. **98,** 207601 (2007).

[45] The phenomenological model of Eq. (2) can be generalized to asymmetric FTJs, as detailed in Supplemental Material [36], Sec. S7.

[46] Y. Hikita, M. Nishikawa, T. Yajima, and H. Y. Hwang, Phys. Rev. B **79,** 073101 (2009).

[47] K. Momma and F. Izumi, J. Appl. Crystallogr. **44,** 1272 (2011).